

Visualizing RNA Extrusion and DNA Wrapping in Transcription Elongation Complexes of Bacterial and Eukaryotic RNA Polymerases

Claudio Rivetti^{1*}, Simone Codeluppi¹, Giorgio Dieci¹ and Carlos Bustamante^{2,3}

¹Department of Biochemistry and Molecular Biology, University of Parma, 43100 Parma, Italy

²Department of Molecular and Cell Biology, University of California, Berkeley, CA 94720 USA

³Department of Physics, Howard Hughes Medical Institute, University of California, Berkeley, CA 94720 USA

Transcription ternary complexes of *Escherichia coli* RNA polymerase and yeast RNA polymerase III have been analyzed by atomic force microscopy. Using the method of nucleotide omission and different DNA templates, *E. coli* RNAP has been stalled at position +24, +70 and +379 and RNAP III at position +377 from the starting site. Conformational analysis of *E. coli* RNAP elongation complexes reveals an average DNA compaction of 22 nm and a DNA deformation compatible with $\sim 180^\circ$ DNA wrapping against the enzyme. The extent of protein–DNA interaction attributed to wrapping, however, is less than that of corresponding open promoter complexes. DNA wrapping was also observed for RNAP III elongation complexes, which showed a DNA compaction of 30 nm. When the RNA polymerases were stalled far from the promoter (+379 and +377), the growing RNA transcript was often visible and it was prevalently seen exiting from the enzyme on the opposite side relative to the smallest angle subtended by the upstream and downstream DNA arms. Surprisingly, we found that many complexes had a second RNAP, not involved in transcription, bound to the growing RNA of a ternary complex. DNA wrapping in the elongation complex suggests a possible mechanism by which the polymerase may overcome the physical barrier to transcription imposed by the nucleosomes.

© 2003 Elsevier Science Ltd. All rights reserved

*Corresponding author

Keywords: atomic force microscopy; DNA wrapping; DNA bending; RNA polymerase; transcription elongation

Introduction

In all cellular organisms, RNA is synthesized by DNA-dependent RNA polymerases (RNAP). These multi-subunit enzymes are responsible for promoter binding, DNA melting, RNA chain initiation, processive elongation, and termination. The bacterial RNAP has a catalytically active core with a subunit composition $\alpha 2\beta\beta'\omega$, aided by a σ factor in promoter recognition and transcription initiation. In eukaryotes there are three different RNA polymerases (RNAP I, II and III), each transcribing a different class of genes. Although their composition comprises more than 12 subunits, the

catalytically competent core of eukaryotic RNAPs is highly conserved in sequence, structure and function and resembles that of bacterial polymerases.^{1–5} Recent crystallographic studies have further emphasized these similarities.^{6–8}

The high resolution crystallographic structures of the bacterial RNAP core and holo enzymes,^{9–11} together with the structure of a holoenzyme–DNA complex¹² have greatly improved our knowledge of the three-dimensional organization of this polymerase and detailed structural models, based on DNA footprinting, protein–DNA and protein–RNA cross-linking and fluorescence resonance energy transfer data, have been proposed to predict the conformation of the open promoter and elongation complexes.^{8,13–16} A step forward has been made in the case of yeast RNAP II for which a 3.3 Å structure of the elongation complex has been determined.⁷ Both bacterial and eukaryotic RNA polymerases have a shape resembling a crab

Abbreviations used: RNAP, RNA polymerase; AFM, atomic force microscopy; Pol, polymerase; EC, elongation complex.

E-mail address of the corresponding author: rivetti@unipr.it

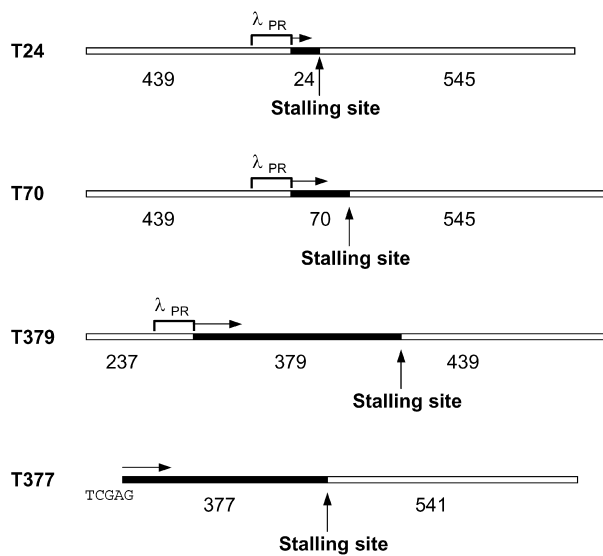


Figure 1. Schematic representation of the DNA templates used in this study. The transcribed region is marked in dark. The promoter region, the direction of transcription and the stalling site are also indicated. The number of base-pairs of the upstream, downstream and transcribed regions are indicated below each template. For T377 the 3' overhang sequence obtained by restriction digestion with *Sac*I endonuclease is also shown.

claw with the two pincers defining a central cleft where the active site is located. In elongation complexes the transcription bubble and the surrounding DNA lie within the cleft with a consequent highly bent conformation of the DNA backbone. The growing RNA transcript is extruded from the elongating enzyme through an exit channel and contacts with the RNAP are maintained up to position around 14–16 nt from the 3' end.^{17–19} A second region of contact between the RNA chain and the polymerase, spanning from position 30 to position 45, has also been suggested.²⁰

Although the nucleic acid structure is well defined within the active-center cleft of the polymerase (Pol) II enzyme, the electron density map of the upstream and downstream DNA is weak and detailed DNA–Pol II interactions made in these regions are not resolved. The short DNA template used and possible crystal packing forces may contribute to the lack of this structural information.⁷

New insights into the structure of the open promoter and elongation complexes also came from high resolution microscopy studies. Both the electron microscope (EM) and the atomic force microscope (AFM) make it possible to look at the global conformation of protein–nucleic acid complexes and can provide information about the spatial relationships between protein, DNA and RNA during transcription elongation.^{21–23} In particular, the AFM offers a number of advantages over other types of microscopes. First, sample deposition in the AFM can be controlled and carried out in relatively mild conditions. Second, samples can be imaged without the aid of contrast agents

at high or low humidity and in a variety of salt conditions. Third, DNA molecules of any arbitrary size can be used. Finally, as with other single molecule visualization methods, AFM studies yield not only the mean of a molecular parameter but also the overall distribution. Since these deviations from the mean represent excursions in the potential energy surface in the parameter space of the molecules, they contain important information as to the nature of the potential energy surface (for a detailed description of the AFM operation mode see review by Bustamante & Rivetti and references therein).²⁴

An AFM study of open promoter complexes of *Escherichia coli* RNAP revealed a significant compaction of DNA upon protein binding.²⁵ Even though the resolution of the microscope was not sufficient to visualize the path of DNA through the protein, this compaction was interpreted as the result of DNA wrapping around the enzyme. This suggestion has been since confirmed by a systematic site-specific protein–DNA photo-cross-linking study in which a similar DNA compaction has been observed in the interaction between the RNAP and the promoter DNA.¹⁵ Furthermore, the crystallographic structure of the bacterial holoenzyme reveals many Mg^{2+} forming a coat on the surface of the protein that could be important in wrapping the DNA around the RNAP during transcription.¹⁰

Based on a number of experimental observations made on prokaryotic and eukaryotic transcription, Coulombe & Burton²⁶ have proposed a DNA wrapping model for the elongation complex as well. In elongation complexes, DNA wrapping and the formation of the RNA–DNA hybrid, may promote the unwinding of the double helix and the maintenance of the transcription bubble. More recently, a photo-crosslinking study of stalled elongation complexes of RNAP II, initiated on a dC-tailed template, have further confirmed this hypothesis, showing a large contact between the RNAP and upstream DNA regions that may lead to DNA wrapping against the RNAP.²⁷

In addition to wrapping and bending of DNA, there are still a number of unresolved issues concerning the way in which the RNA polymerase processively transcribes long stretches of DNA. In particular, much has been speculated about the movement of the RNAP along the DNA *in vivo*, i.e. does it rotate around the DNA as it proceeds or is the enzyme rotationally constrained so that the DNA must swivel around the helical axis as it is threaded through the protein? How is the entanglement of the growing RNA chain with the DNA template prevented? Finally, in the case of eukaryotic RNA polymerases, the way in which the enzyme translocates along the DNA in the presence of the physical barrier imposed by nucleosomal DNA, continues to be an intriguing problem.^{28–30}

Here we present a study based on the AFM visualization of elongation complexes of *E. coli*

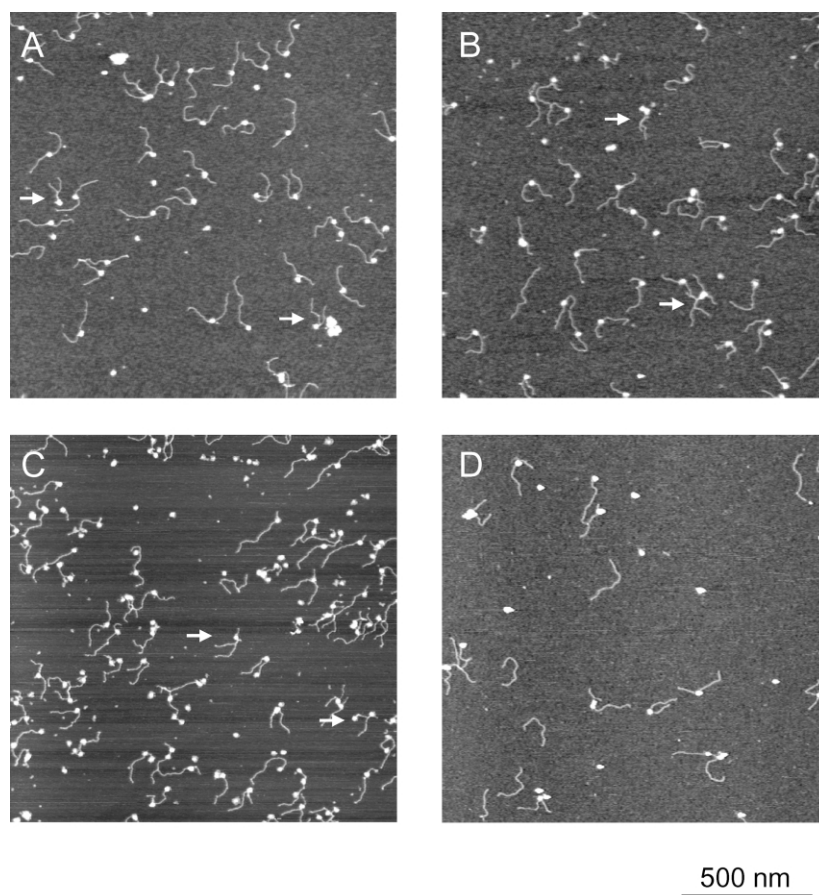


Figure 2. Atomic force microscopy images of stalled elongation complexes. The RNAP molecules are seen as white dots. (A) Image of bacterial EC24 complexes. Stalled ternary complexes are those in which the RNAP is bound near the center of the template. (B) Image of bacterial EC70 complexes. Stalled ternary complexes can be identified as in A. (C) Image of bacterial EC379 complexes. In a few complexes the RNA chain exiting from the polymerase is also visible. In these complexes the upstream DNA corresponds to the longer DNA branch. (D) Image of EC(PIII)377 complexes. Because of the less efficient initiation from the 3' overhang, the number of ternary complexes in each image is small compared to the bacterial RNAP. Arrows point to complexes in which the RNAP is at the apex of plectonemic conformations. All images were recorded in air with the microscope operating in tapping mode. Image sizes are indicated by the bar. The color code corresponds to a height range of 5 nm from dark to clear.

RNAP and *Saccharomyces cerevisiae* RNAP III stalled at different positions by nucleotide omission. This study shows that the DNA is indeed wrapped against the polymerase during transcription elongation, and that the growing RNA transcript is extruded from the protein away from the DNA. We discuss several possible biologically relevant implications of these findings.

Results

AFM of RNAP stalled elongation complexes

AFM imaging of stalled elongation complexes was conducted on four different DNA templates in which the RNA polymerase can be stalled by nucleotide omission (Figure 1). Three of these templates (T24, T70 and T379) harboring a λ_{PR} promoter are specific for *E. coli* RNAP and have the stalling site located at different distances from the start site. The fourth template (T377) is suitable for the assembly of stalled elongation complexes of RNAP III by allowing the polymerase to initiate in a factor-independent manner at the 3' extension of one DNA terminus.³¹ In addition, templates T24 and T70 contain C-less cassettes designed to present identical sequences to the RNAP bound at the stalling site (positions 24 and 70, respectively). Templates T379 and T377 contain similar G-less

cassettes, differing only by two nucleotides at the 5' end, and possess an identical DNA sequence downstream of the stalling site. In all templates, the position of the stalling site is asymmetric within the DNA fragment to facilitate the identification in the images of the upstream and downstream DNA relative to the stalling site. From here on, the corresponding stalled elongation complexes will be referred to as EC24, EC70, EC379 and EC(PIII)377.

E. coli RNAP and RNAP III stalled elongation complexes were assembled in solution under slightly different conditions as described in Materials and Methods and deposited onto freshly cleaved mica in low ionic strength buffer. All images were recorded "in air" using tapping mode AFM. Representative images of EC24 (A), EC70 (B), EC379 (C) and EC(PIII)377 (D) ternary complexes are shown in Figure 2. The concentration of the components and the deposition time were adjusted to have isolated and well-distinguishable molecules over the surface. RNA polymerases located at positions other than the expected stalling site correspond to non-specific complexes, or to elongation complexes arrested within the C-less or G-less cassette: these complexes were not considered in the analysis. Visual inspection of the images reveals three types of RNAP–DNA complexes: (i) those in which the RNAP is stalled at the correct site but the RNA is

Table 1. Types and number of elongation complexes visualized

	RNA not visible	RNA visible	Two RNAP bound	Kinked complexes	RNA entangled with DNA
EC24	913	0	0	38	0
EC70	584	0	0	30	0
EC379	373	235	53	34	1
EC(PIII)377	768	82	168	61	1

Among all AFM images, several types of elongation complexes have been visualized. See the text for description. Column 3 refers to complexes in which a second RNAP, not involved in transcription, is bound to the growing RNA. Kinked complexes are those in which the bend angle is more than 150°.

not visible. This is always the case for EC24 and EC70, whereas for EC379 and EC(PIII)377 the number of complexes in which the RNA is not visible is variable (possibly due to a folded conformation of the RNA, to extended interaction of the RNA with the polymerase, or to loss of the transcript). (ii) Those in which the RNA transcript emerging from the protein is extended and clearly visible. These complexes were found only in EC379 and EC(PIII)377. (iii) Elongation complexes in which the RNA transcript emerging from the elongating RNAP is bound by one or more free RNAP molecules. These structures are peculiar to elongation complexes with a long transcript, since they have never been observed in images of open promoter complexes nor of complexes with a transcript of 24 or 70 nt. Among the many images analyzed, some ternary complexes display kinked structures in which the DNA upstream and downstream of the stall site is supercoiled, forming a slip-knot in which the RNAP is located (complexes indicated by an arrow in Figure 2). Only in a very few cases was the RNA seen entangled with the DNA template. In Table 1, the number of complexes found for each type are reported.

DNA contour length

Comparison of the DNA contour length between free DNA molecules and stalled elongation complexes can provide information on the extent of DNA that makes contact with the protein. In a previous study, measurements of *E. coli* RNAP open

promoter complexes revealed a significant compaction of the apparent DNA contour length induced by the binding of the RNAP, suggesting wrapping of the DNA around the enzyme.²⁵ In Figure 3 the contour length distributions of both *E. coli* RNAP and RNAP III elongation complexes are plotted together with the corresponding contour length of free DNA molecules. The mean contour length of free DNA molecules measured from AFM images is always smaller than the theoretical B-form DNA value corresponding to the canonical rise/bp of 3.4 Å. This effect could be attributed to several factors, such as the drying step of the deposition process, the resolution of the microscope, the algorithm used for computing the contour length.³² Thus, for comparison purposes and whenever possible, measurements of free DNA molecules and elongation complexes have been carried out from the same set of images.

The contour length distributions and the mean values of the Gaussian fitting shown in Table 2, clearly show a significant compaction of the apparent contour length of the DNA in elongation complexes of both bacterial and yeast RNA polymerases. For *E. coli* RNAP the reduction of the DNA contour length is 19, 22 and 26 nm for EC24, EC70 and EC379, respectively. These values must be compared with the 30 nm compaction observed for open promoter complexes on templates T24 and T70.²⁵

Analysis of DNA bend angles

The bend angle distributions, obtained by drawing tangents at the entry and exit points of the DNA from both polymerases, are shown in Figure 4(A)–(D). The distributions share common features: they are wide, the mean values obtained from the Gaussian fitting are similar and all distributions show a group of complexes with bend angles close to 180°, revealing the presence of very kinked structures. The mean values and standard deviation of the distributions are shown in Table 3.

In the case of *E. coli* RNAP elongation complexes, the DNA bend angle was also measured by circular permutation assay. Only T24 and T70 templates were used in this analysis, because the short transcript should not interfere with the mobility of the complex through the gel matrix. For each template two different complexes were

Table 2. Contour length of DNA and elongation complexes

	Free DNA (nm)	EC (nm)	DNA compaction (nm)	No. of DNA molecules	No. of EC
EC24	331 ± 12	312 ± 26	19	947	913
EC70	329 ± 12	307 ± 31	22	302	584
EC379	344 ± 18	318 ± 28	26	211	608
EC(PIII)377	300 ± 10	270 ± 22	31	988	850

The DNA contour length values are the mean of the Gaussian fit of the distributions reported in Figure 3 ± the SD from the mean. The DNA compaction is the difference between the contour length of free DNA molecules and that of elongation complexes. A total of 2448 DNA molecules and 2955 elongation complexes have been measured.

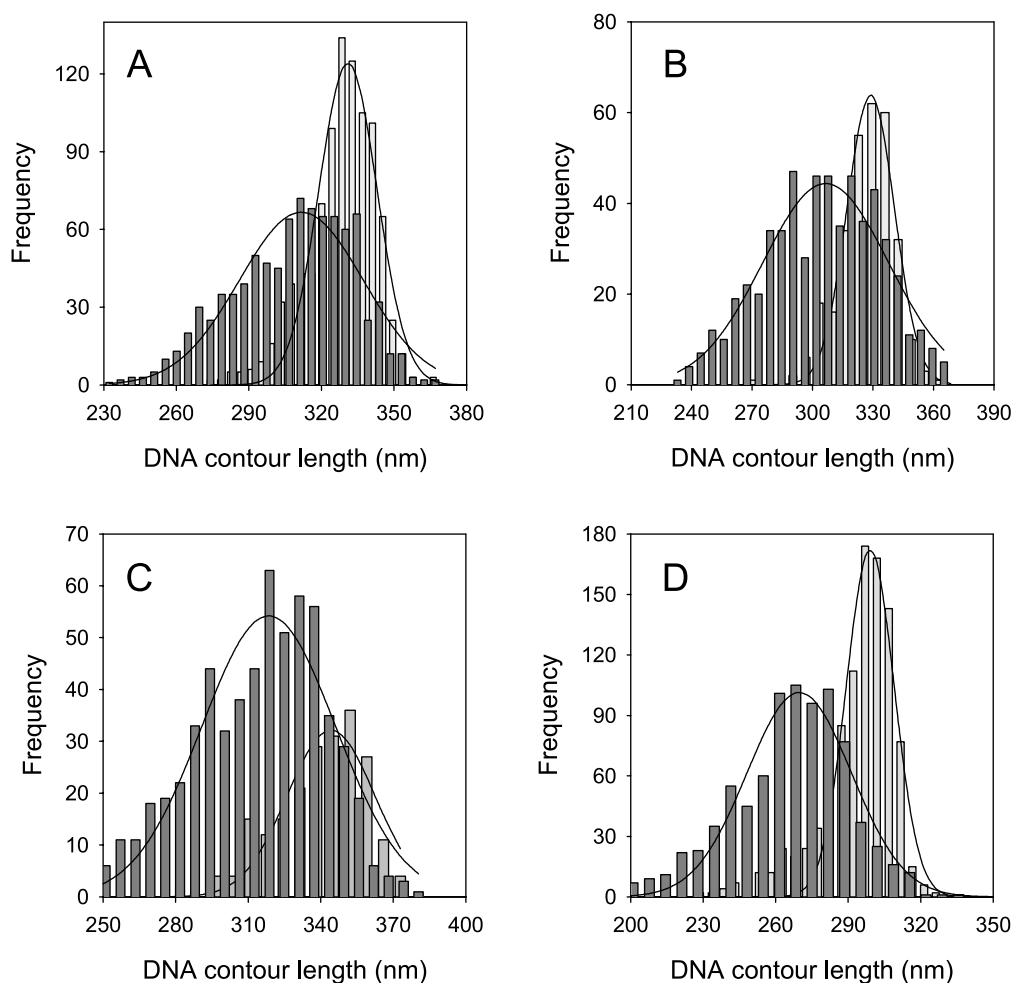


Figure 3. Contour length distributions of free DNA molecules (clear bars) and stalled elongation complexes (dark bars). In all panels the number of bins was determined by the square root of the number of complexes. The lines represent the Gaussian fitting of the distribution and the values obtained from the fitting are shown in Table 2. (A) Bacterial EC24 complexes. (B) Bacterial EC70 complexes. (C) Bacterial EC379 complexes. (D) EC(PIII)377 complexes.

made in which the RNAP was stalled either in the middle or close to the end of a 350 bp DNA fragment. While the DNA fragments displayed the same mobility in the absence of RNAP (data not

shown), indicating the lack of intrinsic DNA bending, a significant lower mobility was observed for the “middle” EC (Figure 4(E), lanes 1 and 3) with respect to the “end” EC (Figure 4(E), lanes 2 and 4). The bend angle was determined using calibration curves obtained with a set of DNA fragments harboring phased A-tracts.³³ The data obtained by circular permutation are summarized in Table 3. The interpretation of the gel mobility results changes depending on the bend angle attributed to each A-tract. If the value of 14° per A-tract, as determined by AFM,³⁴ is used, a bend angle of $87(\pm 2)^\circ$ and $81(\pm 2)^\circ$ is obtained for EC24 and EC70, respectively. Conversely, using the value of 18° per A-tract,³³ a bend angle of $112(\pm 2)^\circ$ and $104(\pm 2)^\circ$ is obtained for EC24 and EC70, respectively (Table 3). The standard deviation reflects the variability within ten independent experiments.

Table 3. DNA bend angles of elongation complexes

	AFM			Gel mobility (deg.)	
	Average (deg.)	Gaussian fit (deg.)	No. of EC	14°	18°
EC24	68 ± 40	55 ± 45	913	87 ± 2	112 ± 2
EC70	77 ± 41	67 ± 50	584	81 ± 2	104 ± 2
EC379	70 ± 43	54 ± 53	608	–	–
EC(PIII)377	72 ± 46	49 ± 63	850	–	–

Bend angle values determined by AFM are given as the average of the sample \pm SD (column 1) and as the mean of the Gaussian fit of the bend angle distributions shown in Figure 4 \pm SD (column 2). In gel mobility shift assays, the DNA bend angle was determined from calibration curves obtained with A-tract markers assuming either 14° or 18° bending for each A-tract. The values are the mean \pm SD of ten independent experiments.

A slightly different gel mobility is observed between EC24 and EC70 end complexes with EC70 running slower than EC24. Since this mobility difference is only observed for the end

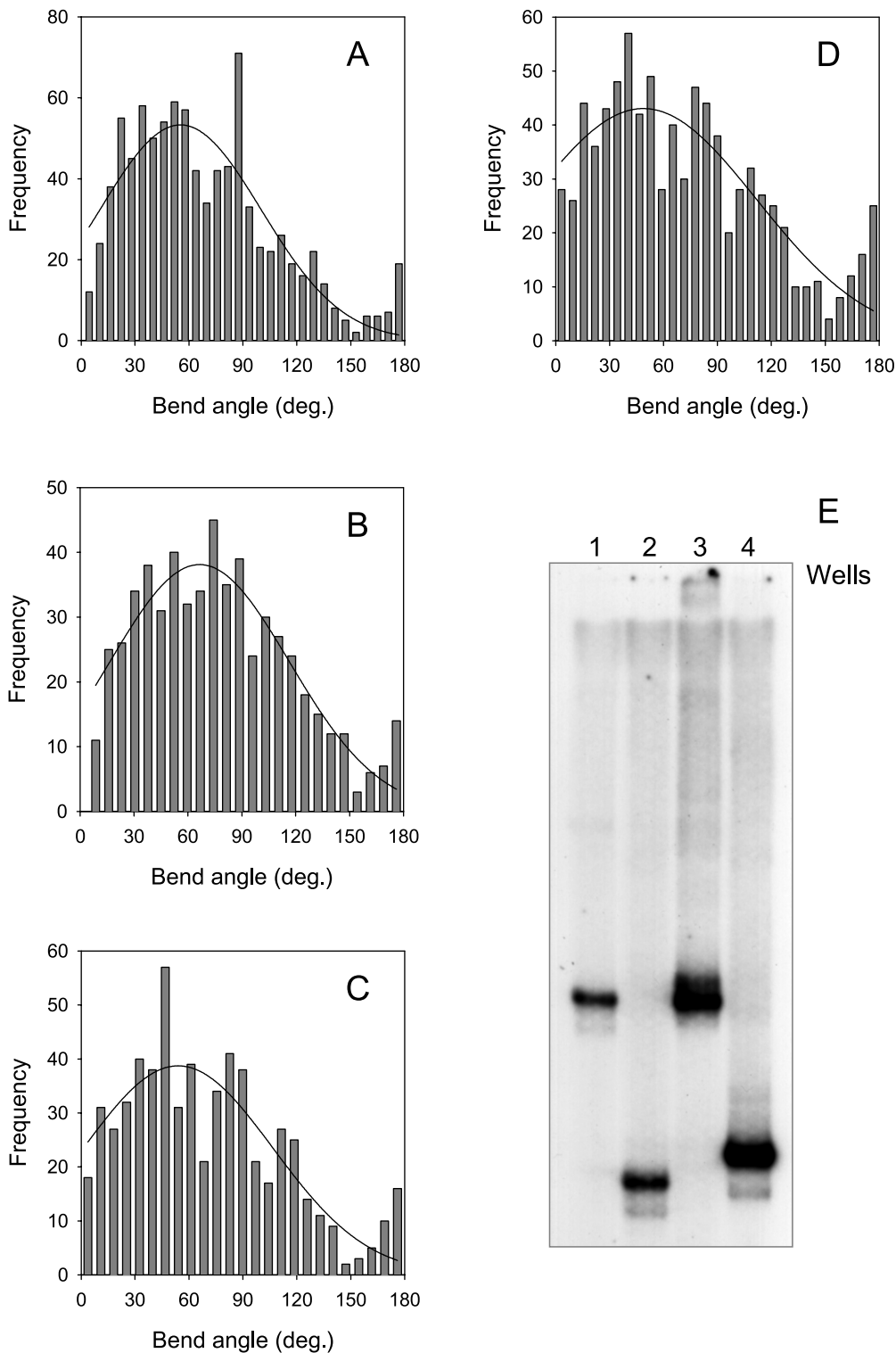


Figure 4. DNA bend angle of stalled elongation complexes. The bend angle distributions shown in A–D were determined by drawing tangents at the entry and exit points of the DNA from the polymerase. In all cases the number of bins is the square root of the number of complexes. The lines represent the Gaussian fitting of the distribution and the values obtained from the fitting are shown in Table 3. (A) Bacterial EC24 complexes. (B) Bacterial EC70 complexes. (C) Bacterial EC379 complexes. (D) EC(PIII)377 complexes. (E) Gel mobility assay of bacterial stalled elongation complexes. The complexes were assembled with 350 bp DNA fragments of templates T24 and T70. In lane 1 and 2 are EC24 complexes stalled in the middle and at the end of the DNA fragment, respectively. In lanes 3 and 4 are EC70 complexes stalled in the middle and at the end of the DNA fragment, respectively. The slightly different migration observed for the two end complexes is probably due to the different size of the RNA chain. For the middle complexes the migration is governed by the bend and the transcript effect is cancelled. The DNA bend angle is determined from calibration curves obtained as described in the text. Bend angles values are shown in Table 3.

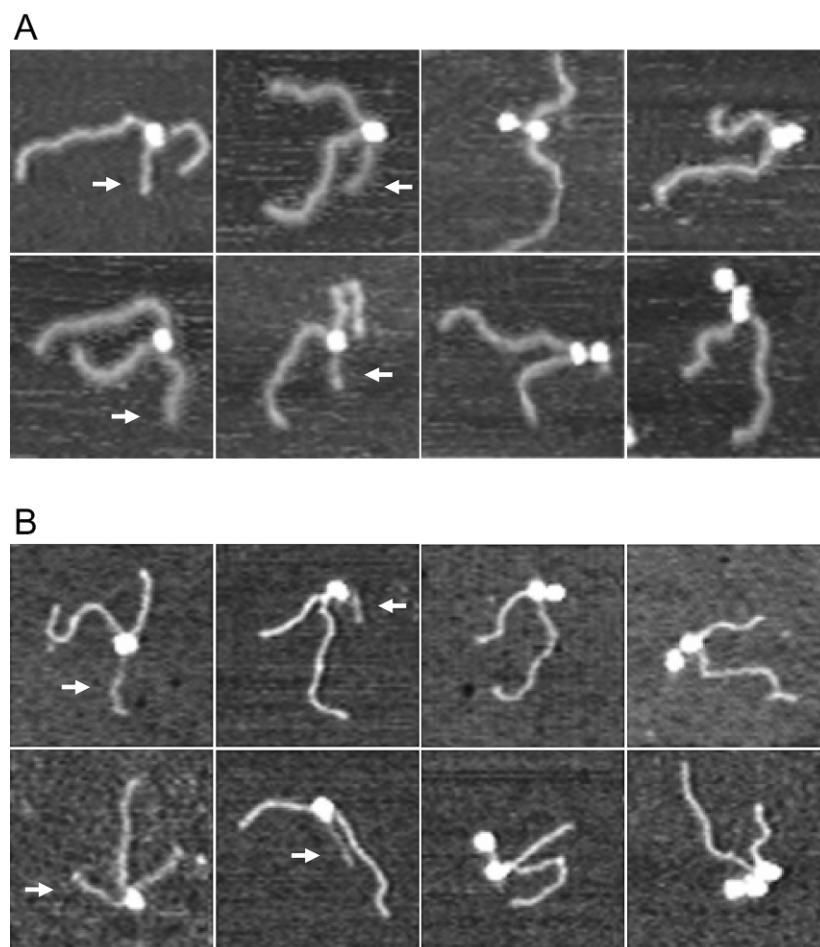


Figure 5. Montage of selected stalled elongation complexes. (A) Ternary complexes of *E. coli* RNAP with template T379. The nascent RNA is indicated by an arrow and the longer branch corresponds to the upstream DNA. Ternary complexes with one or more RNAPs bound to the nascent RNA are shown on the right side. (B) Ternary complexes of RNAP III with template T377. The nascent RNA is indicated by an arrow and the longer branch corresponds to the downstream DNA. Ternary complexes with one or more RNAPs bound to the nascent RNA are shown on the right side. In most complexes, the orientation of the transcript or the position of the second RNAP bound to it, indicate that the RNA is extruded from the RNAP on the outside of the smallest angle subtended by the upstream and downstream DNA.

complexes, where the migration velocity is only related to the molecular mass of the complex, it is most likely due to the longer RNA transcript carried by EC70 and not to a difference in DNA bend angle between the two complexes.

Orientation of the RNA transcript

An important structural information that can be obtained from the visualization of elongation complexes is the location of the exit point of the RNA transcript from the polymerase. In many of the EC379 and EC(PIII)377 imaged, the RNA is clearly visible and its orientation with respect to upstream and downstream DNA can be mapped. Figure 5 displays selected elongation complexes of both bacterial and yeast polymerases. As it can be inferred from Figure 1(C), in elongation complexes of *E. coli* RNAP (Figure 5(A)) the longer branch, the intermediate branch, and the shorter thinner branch emerging from the RNA polymerase, correspond to the upstream DNA, downstream DNA and transcript RNA, respectively. In several of these complexes the emerging RNA transcript is hidden by the binding of one or more RNAPs not engaged in transcription. In this case, the RNAP engaged in transcription is assumed to be the one that makes more contacts with the DNA. From a

visual inspection of the complexes in Figure 5(A) it appears that the RNA exit point is predominantly located on the opposite side of the RNAP with respect to the smaller angle formed by the two DNA arms. In fact, out of 235 complexes measured, only 54 (23%) had the RNA exiting inside the angle formed by the upstream and downstream DNA arms.

In the case of yeast RNAP III (Figure 5(B)), the different design of template T377 identifies the longer branch, the intermediate branch, and the shorter thinner branch emerging from the polymerase, as the downstream DNA, upstream DNA and transcript RNA, respectively. Here, once again, the RNA exit point appears to be predominantly located on the opposite side of the RNA polymerase with respect to the smaller angle formed by the two DNA arms. Out of 82 complexes, only seven (9%) had the RNA positioned within the smaller angle formed by the upstream and downstream DNA arms.

Using the upstream DNA as a reference and projecting it beyond the enzyme, a positive bend angle is defined arbitrarily as that which takes this projection onto the downstream DNA segment *via* a clockwise movement. Then, complexes with negative bend angles are assumed to be adsorbed onto the surface in a bottom up orientation³⁵ and have

been algebraically flipped. The position of the RNA transcript has been defined by measuring two complementary, yet not redundant, angles: one is the positive angle between the upstream DNA and the RNA measured in a clockwise direction from the former to the latter, the other is the positive angle between the downstream DNA and the RNA measured in a clockwise direction from the former to the latter. The two angle distributions obtained can contain independent structural features, given the fact that the bend angle does not have a fixed value.

The results of the DNA–RNA angle measurements are shown in Figure 6. From the angle distribution of *E. coli* RNAP complexes (Figure 6(A) and (B)), two populations are visible: one in which the emerging RNA forms an angle of about 140° with the upstream DNA and the other, less frequent, in which the DNA–RNA angle is of about 280°. For RNAP III (Figure 6(E) and (F)) the RNA exits the protein with an angle of about 110° from the upstream DNA. Combining these data with the bend angle values, the schematic representations shown in Figure 6(C) and (F) can be drawn.

To further investigate the observation made in several AFM images where a second RNAP was bound to the nascent transcript, we have analyzed the ability of *E. coli* RNAP and RNAP III to bind free RNA by filter binding assay. The experiment has been performed with radiolabeled RNA as a probe and BSA and lysozyme as control proteins (data not shown). The results show that both bacterial and yeast RNA polymerases can readily bind free RNA and their affinity is maintained also at the salt concentration at which the elongation complexes are assembled. This excludes the possibility that double-RNAP complexes were caused by the low salt condition used in the sample deposition prior to AFM imaging. While BSA has no affinity for RNA, a basic protein-like lysozyme binds RNA although the binding is more salt-sensitive compared to that of the RNA polymerases.

A second evidence in support of the ability of RNAP to bind RNA comes from the observation that the length of the transcript, even though variable among the different complexes, is always shorter than the contour length of the transcribed DNA region (Figure 5). This feature is particularly evident in the case of the EC(PIII)377 in which the transcribed DNA region coincides with the shorter DNA arm. In addition, the RNA transcript is never visible in elongation complexes with a 70 nt transcript (EC70). Crosslinking and RNase protection experiments^{17–19} indicate that the RNA transcript contacts the RNAP up to nucleotide 14–16 from the growing 3′ end although other studies have found contacts with the polymerase in regions after position 16.^{20,36} The short transcripts observed in the images could be an indication of such interaction. Alternatively, the RNA chain could be in a non-random coil configuration, attaining a secondary structure with a smaller

rise/nt that is responsible for the apparent short transcripts.

Discussion

Understanding the structural–functional relationships of transcription is essential to a comprehensive picture of gene expression. Recent advances in the structural characterization of bacterial and yeast RNA polymerases have been a major step in this direction. Here we have shown how AFM visualization of stalled elongation complexes can reveal structural features that are not easily seen with other techniques. The main advantage comes from the possibility of using long DNA fragments that can better reproduce the full-set of interactions between the elongating enzyme and the DNA template. Even though the resolution of the microscope does not allow a direct mapping of the trajectory of the DNA within the protein core, a detailed analysis of the DNA contour length suggests that DNA wraps against the RNAP in elongating complexes.

In a previous AFM study we have shown that formation of the OPC at the λ_{PR} promoter results in a DNA compaction of about 30 nm consistent with an $\sim 300^\circ$ DNA wrapping against the RNAP.²⁵ Such a degree of compaction is compatible with the model proposed by Naryskin *et al.*¹⁵ where DNA bending, DNA kinking and extended interactions of the upstream DNA (from –43 to –93) with the C-terminal domains of the α subunits constrain about 110 bp (from +20 to –93) of promoter DNA in contact with the polymerase. The ~ 22 nm average DNA compaction observed for the *E. coli* RNAP elongation complexes analyzed here, suggests a less extensive, as compared to initiation complexes, DNA wrapping ($\sim 180^\circ$). This less strong compaction and reduced wrapping likely results from a loss of contacts between the polymerase and the DNA during the transition from initiation to elongation. Since in OPCs a major contribution to wrapping derives from sequence-specific contacts with the region upstream of the promoter, it is conceivable to imagine that some of these interactions are lost upon switching to elongating complexes. This interpretation is in keeping with the reduction of the DNA footprinting observed in the transition from OPC to EC.^{37,38} However, while an ~ 22 nm DNA compaction indicates a protein–DNA contact that spans about 60 bp, footprinting data point to an interaction involving no more than 35 bp. In the case of RNAP III, the observed DNA compaction of elongation complexes is higher relative to the bacterial RNAP, with an average value of about 30 nm. The larger size of RNAP III (~ 700 kDa) and a larger protein–DNA interaction in the upstream region³⁹ can both account for the increased DNA compaction observed in these complexes.

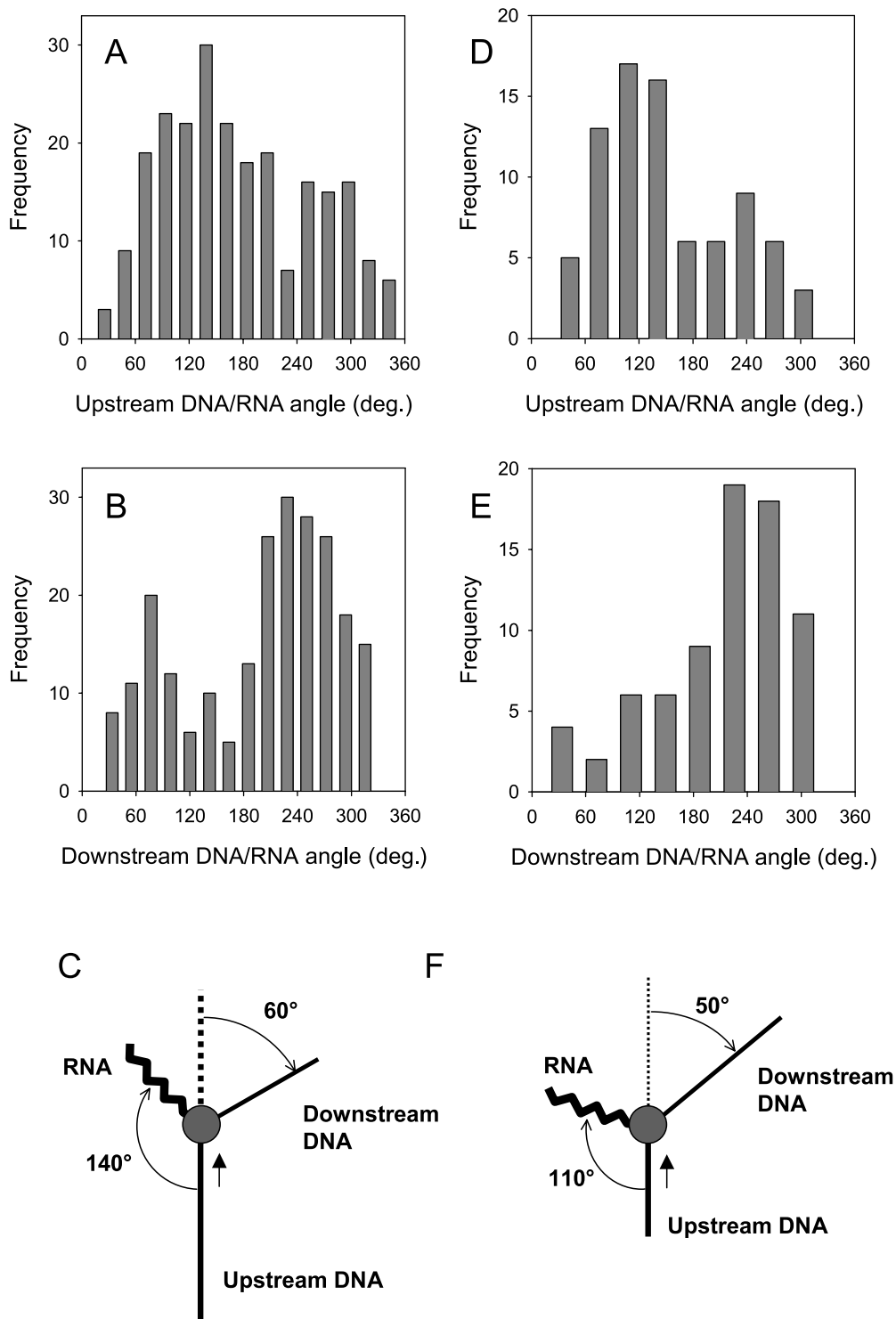


Figure 6. Orientation of the RNA transcript relative to the ternary complex. Within the complex, the exit point of the RNA from the polymerase has been determined by measuring the angle it formed with both the upstream and downstream DNA (see the text for details). (A), (B) Angle distributions for the bacterial EC379 complexes. (D), (E) Angle distributions for the EC(PII)377 complexes. In accordance with the bend angle and the RNA orientation measurements, a schematic representation of the bacterial RNAP (C) and RNAP III (F) ternary complexes are drawn. The DNA is indicated by the thin line, the polymerase is indicated by the circular object and the RNA by the thick wiggled line. The direction of transcription is indicated by an arrow. Upstream and downstream DNA are drawn in scale with DNA templates.

A DNA wrapping of 180° , as inferred from DNA compaction, should correspond to a bend angle of 180° . However, the bend angle distributions obtained with the tangent method, which is independent of contour length measurements, are fairly broad with a peak around 70° . Although these values are somewhat inconsistent, we believe that measurements of DNA bending are more affected by the 3D \rightarrow 2D transition associated with the deposition of the complexes onto the mica surface. Thus, DNA compaction data seem to be a more reliable indicator of the extent of the protein–DNA interaction.

In addition, the bend angle distributions presented in Figure 4 show the existence of highly bent conformations with angles close to 180° . In these complexes the upstream and the downstream DNA is often supercoiled in a plectonemic configuration and the RNAP is found at the apex of the loop with the RNA exiting on the opposite side of the protein relative to the DNA. Similar conformations were observed for transcription complexes assembled on a negatively supercoiled plasmid and their presence was associated with the protein-induced DNA bend angle.²¹ We thus argue that these structures are the result of DNA wrapping against the RNAP, which generates what appears in the images as a highly bent DNA conformation.

The gel mobility of the EC is reduced relative to that of the OPC, suggesting that the bend angle defined by the entry and exit arms of the DNA on both sides of the polymerase is larger in the case of the former complexes. How can this result be reconciled with the loss of contacts between the DNA and the enzyme in EC? Circular permutation assays are based on the different gel migration of protein–DNA complexes located at different positions along the template DNA when subjected to an electric field. Even though not fully understood, this phenomenon is thought to be due to the friction that bent polymers experience as they move within the gel matrix and is therefore highly correlated with their end-to-end distance. Should the DNA in the OPC be wrapped for a complete turn with juxtaposition of upstream and downstream sequences, a decrease of wrapping would produce complexes with a smaller end-to-end distance, i.e. increased gel retardation. Schematically, the conformational changes associated with the transition from an open to an elongation complex can be viewed as the transition from an “ α ” shaped to a “U” shaped complex. As the polymerase proceeds through the transcribed DNA region, it propagates a “bending wave” from the promoter, to the terminator where the energy stored in the DNA deformation might facilitate complex dissociation and transcript release.

Interestingly, this kind of scenario has been envisioned recently for the Pol II elongation complex,^{26,27} which partially resembles the isomerized pre-initiation complex, where the DNA has been speculated to make a full turn around the

polymerase. Based on the sequence and structural similarities among eukaryotic and bacterial RNA polymerases, DNA wrapping may be a common feature of multi-subunit RNA polymerases.

E. coli RNAP stalled elongation complexes, EC24 and EC70, were designed so as to allow that an RNAP, stalled at different distances from the promoter, can contact the same DNA sequence. These complexes were aimed to separate the effect of the DNA sequence from that of the distance traveled by the RNAP on the conformation of a ternary complex. The amount of DNA compaction increases from 19 nm to 22 nm and the DNA bend angle increases from $55(\pm 45)^\circ$ to $67(\pm 50)^\circ$ as the RNAP moves from position +24 to +70 (Tables 2 and 3). These differences, however, are small compared to the variability of the measurements, and we are inclined to conclude that these two ternary complexes have similar conformations. As the polymerase moves further downstream, reaching position +379, the DNA compaction raises to 26 nm, but for these complexes the DNA sequence contacted by the RNAP is different.

One of the advantages of single molecule visualization methods, is their ability to provide the overall distribution of the molecular parameter that is being measured. In the case of bend angle and contour length measurements, the spread of the corresponding distributions, although possibly influenced by other factors,^{24,32} suggests that the interactions responsible for DNA wrapping in the elongation complex are weak. What is not possible to understand from these data, however, is whether these many different observed conformations reflect different states of an active elongation complex or whether they result from the concomitant presence of “active” and “inactive” conformations with different bending properties as proposed by the branched kinetic pathway of transcription elongation.²⁶

In both EC379 and EC(PIII)377, the RNA chain exiting from the RNAP is clearly visible and its location is prevalently mapped on the opposite side of the protein relative to the smaller angle subtended by the DNA arms. The distribution of the angles formed by the upstream DNA and the RNA has a peak around 140° and 110° for bacterial and yeast RNA polymerases, respectively. In the case of *E. coli* RNAP, a secondary peak, centered around 280° in Figure 6(A) and 70° in Figure 6(B), shows that in a significant number of such complexes the exiting RNA is close to the downstream DNA arm. This result is in good agreement with structural and crosslinking data that position the RNA exit site near to the DNA entry site.⁸ The location of the RNA exit site may help in keeping the transcript far away from the DNA arms and could contribute, together with wrapping, to the unhindered growth of the RNA chain.

A more surprising observation made in the images of ternary complexes with long transcripts, is one involving the binding of a second RNAP to the nascent RNA chain. This may be explained by

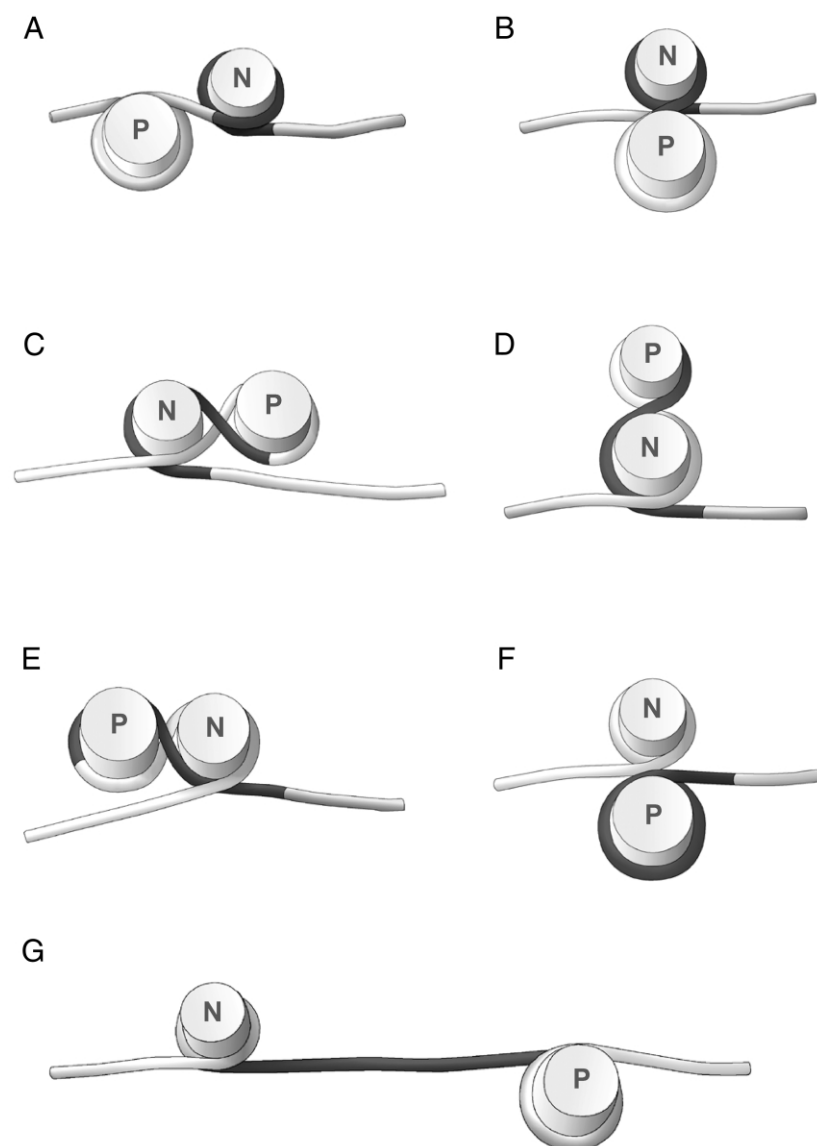


Figure 7. Schematic representation of transcription through a nucleosome. The drawing illustrates a speculative corollary of DNA wrapping in the elongation complex. (A)–(G) The progressing of RNAP (P) through a nucleosome (N); the DNA in contact with the histone octamer is shown in dark. The direction of transcription is from left to right; for clarity reasons, the DNA is represented with only one turn around the histone octamer and the elongation complex is drawn with the juxtaposition of upstream and downstream DNA. However, backward displacement of the histone octamer can also arise from a less extended ($\sim 180^\circ$) DNA wrapping and it is not affected by the number of turns made by the RNAP around the nucleosome. See the text for details.

the existence of an RNA binding site on the bacterial enzyme as reported previously.²⁰ This interaction has been confirmed by filter binding assays conducted on both *E. coli* RNAP and yeast RNAP III. Binding of RNA to the polymerase could increase the local concentration of polymerases in the proximity of transcribed genes, thus functioning as an allosteric transcription regulator.⁴⁰

What are the implications of DNA wrapping in the elongation complex? A left-handed DNA superhelix favors unwinding of the double helix, thus stabilizing the transcription bubble within the polymerase active site. Furthermore, DNA wrapping in transcription elongation may prevent the RNAP from rotating around the DNA, thus favoring swiveling of the DNA while it passes through the protein. With the RNA exiting on the opposite side of the protein relative to the DNA, entangling of the RNA with the DNA is prevented and the transcript can grow unhindered. When transcription approaches termination, the energy stored in

the bent DNA can therefore be utilized for transcript release.

If transferred to a more realistic nucleoprotein context, where chromatin rather than naked DNA is transcribed, DNA wrapping in the elongation complex suggests a speculative, yet interesting scheme describing the movement of an RNA polymerase molecule through a nucleosome. In a series of elegant experiments, Studisky and collaborators^{28,29} showed how transcription by SP6 or RNAP III of a DNA template on which a nucleosome was positioned, caused the histone octamer to move backwards with respect to the direction of transcription without dissociating from the DNA. Based on endonuclease protection patterns these authors obtained an estimate for this movement of about 80 bp (27 nm).

In accordance with the model they proposed, we suggest, here, that the backward movement of the nucleosome is a natural, structural consequence of DNA wrapping in ECs. An exemplifying scheme of this process is shown in Figure 7. A transcribing

RNAP (P) approaches a nucleosome (N) from the left (Figure 7(A)). The nucleosome DNA is shown in dark and, for clarity reasons, it makes only one turn around the histone octamer. When an RNAP encounters a nucleosome (Figure 7(B)), it continues its movement by taking up the downstream DNA from the nucleosome and by giving back the upstream DNA already transcribed (Figure 7(C)–(E)). In our scheme, the RNA polymerase passes through the nucleosome while remaining on the outer surface with no need to form DNA loops because it is the DNA (not the RNAP) that swivels around the helical axis. Such a mode of progression implies that when the RNAP overcomes the nucleosome (Figure 7(F) and (G)), the histone octamer is displaced backwards, relative to its initial position on the DNA. Even though the elongation complex is drawn with the juxtaposition of upstream and downstream DNA, the model is equally valid for a less extended (~180°) DNA wrapping. Importantly, an identical extent of histone octamer displacement is expected to take place in the case of an RNAP making two full-turns around the nucleosome.

Future experiments aimed at visualizing an RNAP while transcribing a DNA template with a positioned nucleosome will help to decipher this puzzle.

Materials and Methods

DNA templates and RNA polymerase enzymes

DNA templates T24 and T70 were obtained by restriction digestion with *Hind*III endonuclease of pDE13 and pSAP plasmids, respectively.²⁵ T379 was obtained by PCR using pNEB-Gless- λ_{PR} plasmid as template, Deep Vent DNA polymerase (New England Biolabs) and oligonucleotide primers (CAGTCACGACGTTGTAAAACG; GCTGGCCTTTTGCTCACATG). T377 was obtained by PCR using pNEB-Gless as template, Deep Vent DNA polymerase and oligonucleotide primers (GAGACGGT CACAGCTTGCTG; GGTATCTTTATAGTCCTGTCGGG), followed by restriction digestion with *Sac*I endonuclease to produce the 3' overhang terminus from which transcription can be initiated. The Gless cassette used to construct these plasmids has been amplified by PCR from pML(C2AT)19 Δ -50 plasmid using Deep Vent DNA polymerase and oligonucleotide primers (GGAATGAGAA ATGAGTGTGAGG; AAGAGCTCTTCCCCTCCATACCC), a kind gift from Michele Sawadogo. All DNA fragments were gel purified on 1% (w/v) agarose gel and recovered by electroelution in an Elutrap apparatus (Schleicher & Schuell, Keene NH). The DNA was phenol–chloroform-extracted, ethanol-precipitated and resuspended in TE buffer (50 mM Tris–HCl (pH 7.4), 1 mM EDTA). The concentration of the DNA was determined by absorbance at 260 nm. *E. coli* RNA harboring a histidine tag in the β' subunit was purified as described,⁴¹ yeast RNAP III was purified as described by Huet *et al.*⁴²

Stalled elongation complexes

EC24 and EC70 stalled elongation complexes of *E. coli* RNAP to be used for AFM imaging were prepared by mixing 200 fmol of DNA template and 200 fmol of

RNAP in 10 μ l of transcription buffer A (20 mM Tris–HCl (pH 7.9), 50 mM KCl, 5 mM MgCl₂, 1 mM DTT) containing 20 units of ribonuclease inhibitor (Rnasin, Promega). After a 15 minute incubation at 37 °C to facilitate open promoter complex formation, a mixture of three nucleotides (ATP, UTP and GTP) was added to the reaction to a final concentration of 100 μ M each. Transcription was carried out at room temperature for 20 minutes and the reaction was immediately used for AFM imaging. EC379 were assembled in similar conditions with the exception that a mixture of ATP, UTP and CTP was used.

EC(PIII)377 stalled elongation complexes were formed in a reaction mixture containing: 200 fmol of DNA, 350 fmol of RNAP III, 400 μ M CpU dinucleotide, 200 μ M ATP, 200 μ M UTP, 200 μ M CTP, 20 units of ribonuclease inhibitor in transcription buffer B (40 mM Tris–HCl (pH 8), 100 mM KCl, 6 mM MgCl₂, 1 mM DDT). The reaction was incubated at 30 °C for 45 minutes.

Gel mobility shift assay

Gel mobility shift assays were performed with DNA fragments of 350 bp obtained from pDE13 and pSAP by PCR using specific primers. For each plasmid two different DNA fragments were obtained: one with the stalling site located near the center of the fragment (middle) and the other with the stalling site located at one end of the DNA fragment (end). All DNA fragments were purified as described above. Stalled elongation complexes were assembled in transcription buffer A using 0.4 pmol of DNA and 1 pmol of *E. coli* RNAP. After a 15 minute incubation at 37 °C, heparin was added to a final concentration of 200 μ g/ml. Then 0.5 μ l of [α -³²P]UTP (6000 Ci/mmol) and a mixture of ATP, UTP, and GTP, at a final concentration of 20 μ M each, were added to the reaction. Transcription was allowed to take place for about 20 minutes at room temperature. The samples were loaded onto a 4% (37.5:1 acrylamide/bis-acrylamide) non-denaturing polyacrylamide gel. Electrophoresis was carried out in TBE buffer at a constant voltage of 300 V for ten hours. The gel temperature was 11 °C. Gel mobility analysis of DNA fragments without polymerase was performed in the same conditions with an electrophoresis time of four hours. The bend angle calibration curve was determined in identical gel conditions with an electrophoresis time of five hours. Bend angle markers were obtained from plasmids pJT170-3 through pJT170-6 as described by Thompson & Landy.³³ In all cases, migration of the complexes was visualized by autoradiography.

Filter binding assay

A radiolabeled RNA fragment of 366 nt has been obtained by transcribing a linearized pBlueScript-KS construct containing the *S. cerevisiae* I(TAT)LR1 tRNA gene⁴³ with T7 RNA polymerase in the presence of [α -³²P]UTP. RNA binding assays were conducted in reaction mixtures (total volume of 10 μ l) containing RNA at sub-nanomolar concentration and 100 ng of protein in transcription buffer B. The reaction mixture was incubated for 15 minutes at room temperature and 3 μ l of each reaction were spotted onto three separated strips of Hybond-ECL nitrocellulose membrane (Amersham-Biosciences) and let dry for ten minutes. The membranes were then washed with 10 ml of 0.5, 1 and 2 \times transcription buffer B in a rotary shaker for 15 minutes. Radioactivity on

dried strips was revealed and quantified by phosphor-imaging with a Personal Imager FX (Bio-Rad).

Atomic force microscopy

Stalled elongation complexes prepared as described above were diluted to a concentration of 1–2 nM in 20 μ l of deposition buffer (4 mM Hepes (pH 7.4), 10 mM NaCl, 2 mM MgCl₂) and deposited onto freshly cleaved ruby mica (Mica New York, NY). The sample was incubated for about two minutes and then rinsed with water and dried with a weak flux of nitrogen. AFM images were collected in air with a Nanoscope III microscope (Digital Instruments Inc., Santa Barbara, CA) operating in tapping mode. All operations were done at room temperature. Commercial diving board silicon cantilevers (Nanosensor or Olympus) were used. The microscope was equipped with a type E scanner (12 μ m \times 12 μ m). Images (512 \times 512 pixels) were collected with a scan size of 2 μ m at a scan rate varying between two and five scan lines per second. Water was purified in a Nanopure water purification apparatus (Barnstead, Dubuque Iowa). A detailed description of the sample preparation and AFM procedures can be found in Rivetti *et al.*⁴⁴

Image analysis

The AFM images were analyzed using locally written software (Alex). Measurements were performed only on those molecules that were completely visible in the image, that did not have any RNAP bound at the ends and molecules in which the shape was not ambiguous. The DNA path was digitized as described elsewhere.³² The position of the center of the RNAP was manually selected and automatically adjusted at the nearest point on the traced contour line. DNA bend angle measurements were obtained by drawing lines from the center of the polymerase to the entry and exit points of the DNA. By definition, the deviation from linearity of the two lines measures the bend angle. When visible, the RNA transcript was mapped by drawing a line from the center of the RNAP to the emerging point of the RNA from the protein. The direction of bending was obtained by taking the upstream DNA as reference and determining whether the downstream DNA deviated towards the left or towards the right. We have considered positive the bend angle generated by a clockwise rotation of the downstream DNA with respect to the direction of transcription. Complexes with a negative bend angle have been algebraically flipped. The angle between the upstream or the downstream DNA arm and the RNA chain has then been measured in a clockwise direction from zero to 360°. Data have been elaborated using Matlab and graphs have been made with Sigmaplot.

Acknowledgements

We are grateful to Martin Guthold and Simone Ottonello for critical reading and comments on the manuscript, Michele Sawadogo for providing the G-less cassette and Gian Luca Ferrari for help with the drawing in Figure 7. We also thank the Centro Interfacoltà Misura (CIM) of the University of Parma for the Atomic Force Microscope facility.

pDE plasmid was constructed by Dorothy Erie. This work was supported by the Italian Ministry of University and of Scientific and Technological Research (Cofin 2001).

References

1. Sweetser, D., Nonet, M. & Young, R. A. (1987). Prokaryotic and eukaryotic RNA polymerases have homologous core subunits. *Proc. Natl Acad. Sci. USA*, **84**, 1192–1196.
2. Puhler, G., Leffers, H., Gropp, F., Palm, P., Klenk, H. P., Lottspeich, F. *et al.* (1989). Archaeobacterial DNA-dependent RNA polymerases testify to the evolution of the eukaryotic nuclear genome. *Proc. Natl Acad. Sci. USA*, **86**, 4569–4573.
3. Allison, L. A., Moyle, M., Shales, M. & Ingles, C. J. (1985). Extensive homology among the largest subunits of eukaryotic and prokaryotic RNA polymerases. *Cell*, **42**, 599–610.
4. Polyakov, A., Severinova, E. & Darst, S. A. (1995). Three-dimensional structure of *E. coli* core RNA polymerase: promoter binding and elongation conformation of the enzyme. *Cell*, **83**, 365–373.
5. Ebricht, R. H. (2000). RNA polymerase: structural similarities between bacterial RNA polymerase and eukaryotic RNA polymerase II. *J. Mol. Biol.* **304**, 687–698.
6. Cramer, P., Bushnell, D. A. & Kornberg, R. D. (2001). Structural basis of transcription: RNA polymerase II at 2.8 Å resolution. *Science*, **292**, 1863–1876.
7. Gnat, A. L., Cramer, P., Fu, J., Bushnell, D. A. & Kornberg, R. D. (2001). Structural basis of transcription: an RNA polymerase II elongation complex at 3.3 Å resolution. *Science*, **292**, 1876–1882.
8. Korzheva, N., Mustaev, A., Kozlov, M., Malhotra, A., Nikiforov, V., Goldfarb, A. & Darst, S. A. (2000). A structural model of transcription elongation. *Science*, **289**, 619–625.
9. Zhang, G., Campbell, E. A., Minakhin, L., Richter, C., Severinov, K. & Darst, S. A. (1999). Crystal structure of *Thermus aquaticus* core RNA polymerase at 3.3 Å resolution. *Cell*, **98**, 811–824.
10. Vassilyev, D. G., Sekine, S. I., Laptenko, O., Lee, J., Vassilyeva, M. N., Borukhov, S. & Yokoyama, S. (2002). Crystal structure of a bacterial RNA polymerase holoenzyme at 2.6 Å resolution. *Nature*, **417**, 712–719.
11. Murakami, K. S., Masuda, S. & Darst, S. A. (2002). Structural basis of transcription initiation: RNA polymerase holoenzyme at 4 Å resolution. *Science*, **296**, 1280–1284.
12. Murakami, K. S., Masuda, S., Campbell, E. A., Muzzin, O. & Darst, S. A. (2002). Structural basis of transcription initiation: an RNA polymerase holoenzyme–DNA complex. *Science*, **296**, 1285–1290.
13. Nudler, E. (1999). Transcription elongation: structural basis and mechanisms. *J. Mol. Biol.* **288**, 1–12.
14. Darst, S. A. (2001). Bacterial RNA polymerase. *Curr. Opin. Struct. Biol.* **11**, 155–162.
15. Naryshkin, N., Revyakin, A., Kim, Y., Mekler, V. & Ebricht, R. H. (2000). Structural organization of the RNA polymerase-promoter open complex. *Cell*, **101**, 601–611.
16. Mekler, V., Kortkhonjia, E., Mukhopadhyay, J., Knight, J., Revyakin, A., Kapanidis, A. N. *et al.* (2002). Structural organization of bacterial RNA

- polymerase holoenzyme and the RNA polymerase-promoter open complex. *Cell*, **108**, 599–614.
17. Monforte, J. A., Kahn, J. D. & Hearst, J. E. (1990). RNA folding during transcription by *Escherichia coli* RNA polymerase analyzed by RNA self-cleavage. *Biochemistry*, **29**, 7882–7890.
 18. Komissarova, N. & Kashlev, M. (1998). Functional topography of nascent RNA in elongation intermediates of RNA polymerase. *Proc. Natl Acad. Sci. USA*, **95**, 14699–14704.
 19. Hanna, M. M., Yuriev, E., Zhang, J. & Riggs, D. L. (1999). Probing the environment of nascent RNA in *Escherichia coli* transcription elongation complexes utilizing a new fluorescent ribonucleotide analog. *Nucl. Acids Res.* **27**, 1369–1376.
 20. Altmann, C. R., Solow-Cordero, D. E. & Chamberlin, M. J. (1994). RNA cleavage and chain elongation by *Escherichia coli* DNA-dependent RNA polymerase in a binary enzyme-RNA complex. *Proc. Natl Acad. Sci. USA*, **91**, 3784–3788.
 21. ten Heggeler-Bordier, B., Wahli, W., Adrian, M., Stasiak, A. & Dubochet, J. (1992). The apical localization of transcribing RNA polymerases on supercoiled DNA prevents their rotation around the template. *EMBO J.* **11**, 667–672.
 22. Rees, W. A., Keller, R. W., Vesenska, J. P., Yang, G. & Bustamante, C. (1993). Evidence of DNA bending in transcription complexes imaged by scanning force microscopy. *Science*, **260**, 1646–1649.
 23. Bednar, J., Studitsky, V. M., Grigoryev, S. A., Felsenfeld, G. & Woodcock, C. L. (1999). The nature of the nucleosomal barrier to transcription: direct observation of paused intermediates by electron cryomicroscopy. *Mol. Cell*, **4**, 377–386.
 24. Bustamante, C. & Rivetti, C. (1996). Visualizing protein–nucleic acid interactions on a large scale with the scanning force microscope. *Ann. Rev. Biophys. Biomol. Struct.* **25**, 395–429.
 25. Rivetti, C., Guthold, M. & Bustamante, C. (1999). Wrapping of DNA around the *E. coli* RNA polymerase open promoter complex. *EMBO J.* **18**, 4464–4475.
 26. Coulombe, B. & Burton, Z. F. (1999). DNA bending and wrapping around RNA polymerase: a “revolutionary” model describing transcriptional mechanisms. *Microbiol. Mol. Biol. Rev.* **63**, 457–478.
 27. Wooddell, C. I. & Burgess, R. R. (2000). Topology of yeast RNA polymerase II subunits in transcription elongation complexes studied by photoaffinity cross-linking. *Biochemistry*, **39**, 13405–13421.
 28. Studitsky, V. M., Kassavetis, G. A., Geiduschek, E. P. & Felsenfeld, G. (1997). Mechanism of transcription through the nucleosome by eukaryotic RNA polymerase. *Science*, **278**, 1960–1963.
 29. Studitsky, V. M., Clark, D. J. & Felsenfeld, G. (1994). A histone octamer can step around a transcribing polymerase without leaving the template. *Cell*, **76**, 371–382.
 30. Kireeva, M. L., Walter, W., Tchernajenko, V., Bondarenko, V., Kashlev, M. & Studitsky, V. M. (2002). Nucleosome remodeling induced by RNA polymerase II: loss of the H2A/H2B dimer during transcription. *Mol. Cell*, **9**, 541–552.
 31. Bardeleben, C., Kassavetis, G. A. & Geiduschek, E. P. (1994). Encounters of *Saccharomyces cerevisiae* RNA polymerase III with its transcription factors during RNA chain elongation. *J. Mol. Biol.* **235**, 1193–1205.
 32. Rivetti, C. & Codeluppi, S. (2001). Accurate length determination of DNA molecules visualized by atomic force microscopy: evidence for a partial B- to A-form transition on mica. *Ultramicroscopy*, **87**, 55–66.
 33. Thompson, J. F. & Landy, A. (1988). Empirical estimation of protein-induced DNA bending angles: applications to lambda site-specific recombination complexes. *Nucl. Acids Res.* **16**, 9687–9705.
 34. Rivetti, C., Walker, C. & Bustamante, C. (1998). Polymer chain statistics and conformational analysis of DNA molecules with bends or sections of different flexibility. *J. Mol. Biol.* **280**, 41–59.
 35. Hansma, H. G., Bezanilla, M., Nudler, E., Hansma, P. K., Hoh, J., Kashlev, M. *et al.* (1997). Left-handed conformation of histidine-tagged RNA polymerase complexes imaged by atomic force microscopy. *Probe Microscopy*, **1**, 127–143.
 36. Hanna, M. M. & Meares, C. F. (1983). Topography of transcription: path of the leading end of nascent RNA through the *Escherichia coli* transcription complex. *Proc. Natl Acad. Sci. USA*, **80**, 4238–4242.
 37. Krummel, B. & Chamberlin, M. J. (1992). Structural analysis of ternary complexes of *Escherichia coli* RNA polymerase. Deoxyribonuclease I footprinting of defined complexes. *J. Mol. Biol.* **225**, 239–250.
 38. Metzger, W., Schickor, P. & Heumann, H. (1989). A cinematographic view of *Escherichia coli* RNA polymerase translocation. *EMBO J.* **8**, 2745–2754.
 39. Bartholomew, B., Durkovich, D., Kassavetis, G. A. & Geiduschek, E. P. (1993). Orientation and topography of RNA polymerase III in transcription complexes. *Mol. Cell. Biol.* **13**, 942–952.
 40. Wassarman, K. M. & Storz, G. (2000). 6 S RNA regulates *E. coli* RNA polymerase activity. *Cell*, **101**, 613–623.
 41. Kashlev, M., Martin, E., Polyakov, A., Severinov, K., Nikiforov, V. & Goldfarb, A. (1993). Histidine-tagged RNA polymerase: dissection of the transcription cycle using immobilized enzyme. *Gene*, **130**, 9–14.
 42. Huet, J., Manaud, N., Dieci, G., Peyroche, G., Conesa, C., Lefebvre, O. *et al.* (1996). RNA polymerase III and class III transcription factors from *Saccharomyces cerevisiae*. *Methods Enzymol.* **273**, 249–267.
 43. Dieci, G., Percudani, R., Giuliodori, S., Bottarelli, L. & Ottonello, S. (2000). TFIIC-independent *in vitro* transcription of yeast tRNA genes. *J. Mol. Biol.* **299**, 601–613.
 44. Rivetti, C., Guthold, M. & Bustamante, C. (2000). DNA wrapping in *E. coli* RNA polymerase open promoter complexes revealed by scanning force microscopy. In *DNA–Protein Interactions* (Travers, A. & Buckle, M., eds), pp. 113–123, Oxford University Press, Oxford.

Edited by R. Ebright

(Received 11 October 2002; accepted 16 December 2002)